Visual Neuroscience (1989), **2**, 297–313. Printed in the USA.
Copyright © 1989 Cambridge University Press 0952-5238/89 $5.00 + .00

Cortical interactions in texture processing: Scale and dynamics

JONATHAN D. VICTOR AND MARY M. CONTE

Department of Neurology, Cornell University Medical College, New York City, and
Laboratory of Biophysics, The Rockefeller University, New York City

(RECEIVED April 26, 1988; ACCEPTED August 23, 1988)

Abstract

We investigate the neural computations underlying pattern processing with stimuli based on textures balanced for spatial frequency content (and second-order correlations) but not for higher-order correlations (Julesz et al. 1978). Interchange between two such isodipole textures produces a robust human visual evoked potential (VEP). The difference in population activity driven by two isodipole textures is quantified by the antisymmetric component of the VEP. Statistical properties of the textures eliminate contributions from linear mechanisms to the antisymmetric VEP.

The dependence of the antisymmetric VEP on check size and fourth-order correlation statistics is used to test nonlinear models for the underlying neural computations. Linear summation, followed by a simple nonlinearity (such as rectification, saturation, or threshold), is inconsistent with the data. More elaborate models, in which a second nonlinear stage combines the output of local nonlinear mechanisms, are consistent with the data, provided that an appropriate spatial scale is chosen for the second stage of processing. For checks 4 min or smaller, the deduced interaction length is 10–15 min. For checks larger than 4 min, the interaction length is proportional to check size.

Keywords: Visual textures, Nonlinear interactions, Visual evoked potentials

Introduction

An important aspect of human visual function is the ability to identify a region of a visual pattern that is different from its milieu. This identification process proceeds rapidly and in parallel, independent of focused attention (Bergen & Julesz, 1983).

Julesz (1962) introduced the texture-discrimination paradigm to study this parallel process. He and others demonstrated that, in many instances, early visual processing is able to segregate textures on the basis of spatial frequency content or, equivalently, second-order correlation; discrimination usually failed if second-order statistics were equal. This kind of performance would be expected from a preattentive visual system that (abstractly) consisted of banks of spatial frequency filters. However, textures with identical second-order statistics were found to be rapidly discriminable if they contained a difference in the density of certain simple feature elements (Julesz, 1981). Rapid discrimination of these isodipole textures implies a more complex picture of the early visual process, perhaps involving the extraction of local features. The goal of this work is to define the spatial extent and dynamics of neural interactions subserving this early stage of visual processing.

Reprint requests to: Jonathan D. Victor, Department of Neurology, Cornell University Medical College, 1300 York Avenue, New York, NY 10021.

Two distinct, statistically homogeneous isodipole textures may differ only in the spatial phases of the individual spatial Fourier components. However, spatial homogeneity implies that the phase of any single spatial Fourier component is meaningless: it depends on the arbitrary choice of a coordinate-system origin. But, once the phase of a particular spatial Fourier component is chosen, phases of other harmonically related Fourier components are constrained. That is, in the spatial-frequency domain, discrimination between isodipole textures is possible only if relative phases of two or more grating components are compared. Whether viewed in the spatial domain or in the spatial frequency domain, the requisite neural computations are nonlinear.

The nonlinear nature of these processes allows separation of cortical computations from those at the retinal and thalamic level. These earlier stages of computation are either linear or contain nonlinearities that are relatively simple and well-characterized. For this reason, differential visual evoked potentials (VEPs) elicited by discriminable isodipole textures provide a window onto cortical interactions (Victor & Zemon, 1985; Victor, 1985, 1986).

Although it is useful to be able to detect such cortical interactions, it would be more desirable to define these interactions in more detail. One issue is the spatial scale of these intracortical interactions. Because the interactions are phase sensitive and appear to detect *local* texture features, these feature-detec-

tion computations are generally thought of as local processes. However, given the highly nonlinear nature of the cortical interactions, separation of local from longer-range interactions is not a simple matter. A related issue is the time course of these interactions, and to what extent these dynamics depend on stimulus complexity.

We have approached these questions by investigating the dependence of the VEP on one basic parameter of the even/odd isodipole stimulus: check size. In addition, we examined the VEP elicited by generalizations of these textures that retain the key isodipole properties. The new textures vary in long-range, high-order correlation statistics without varying in spatial frequency content or local high-order correlation statistics. The simple manipulations allow us to place certain qualitative constraints on a minimally adequate model. The studies involving the new textures lead to hypotheses for the spatial organization of the neural computations.

The stimuli used here, by virtue of their statistical properties, cancel responses that may be simply derived from the retinal output, and thus permit isolation of processes that depend on complex neural interactions. Traditional stimuli, such as spots, bars, and gratings, do not permit a robust separation of complex nonlinear processes from simpler processes, such as linear filtering, rectification, saturation, and threshold. It is hard to imagine that complex neural interactions are driven solely by isodipole textures; rather (see, for example, the models developed in the Discussion), they are likely to be elicited by the traditional stimuli as well. Thus, we view the isodipole texture technique as a means to isolate and study neural computations underlying pattern processing in general.

Methods

Visual stimuli

The main experimental tool is a set of visual textures whose statistical properties facilitate separation of (1) cortical *vs* precortical interactions, and (2) local *vs* long-range interactions. These "even" and "odd" textures (described in detail in Julesz et al. (1978), and referred to here as the "basic" textures) are black-and-white colorings of a square lattice. The first row and first column of the lattice are colored at random; the interior checks are colored according to a fourth-order recursion relation.

In the present study, we also used a generalization of the basic textures. The new textures are constructed from the even and the odd textures by introducing two different kinds of disorder: *propagated* disorder, parametrized by ϵ_{prop}, and sporadic disorder, parametrized by ϵ_{spor}. Together, the two kinds of stochastic processes provide for a large family of isodipole textures. Examples of these textures are shown in Fig. 1.

In the first stage of the construction, an underlying state of $+1$ or -1 is assigned to each square of a lattice. We will denote the state assigned to the check in row i and column j by $a_{i,j}$. The states of checks in the first column, $a_{i,0}$, and the states of checks in the first row, $a_{0,j}$, are chosen in a random, uncorrelated fashion to be -1 or $+1$. In the original textures, states of checks in the interior of the texture are assigned by a deterministic recursion rule

$$a_{i,j} \cdot a_{i-1,j} \cdot a_{i,j-1} \cdot a_{i-1,j-1} = \begin{cases} +1 & \text{(even texture)}, \\ -1 & \text{(odd texture)}. \end{cases} \quad (1)$$

However, in the present generalization, propagated disorder is introduced into the assignment of states to checks in the interior of the texture. This is accomplished by the stochastic recursion rule

$$\text{prob}\{a_{i,j} \cdot a_{i-1,j} \cdot a_{i,j-1} \cdot a_{i-1,j-1} = 1\} = 1 - \epsilon_{\text{prop}}. \quad (2)$$

The parameter ϵ_{prop} is called the "propagated error." For $\epsilon_{\text{prop}} = 0$, the original even texture of Julesz et al. (1978) is recovered. For $\epsilon_{\text{prop}} = 1$, the odd texture of Julesz et al. (1978) is recovered. Intermediate values of the propagated error yield intermediate textures; $\epsilon_{\text{prop}} = 0.5$ yields a completely random texture.

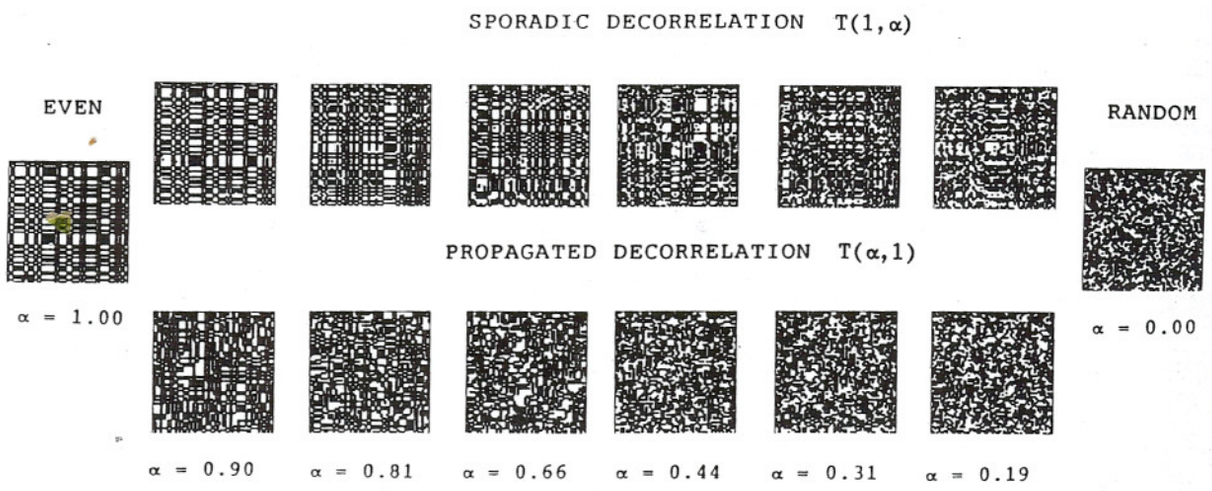

Fig. 1. Examples of the visual textures used in this study. The texture on the extreme left is the basic even texture. The texture on the extreme right is a random texture. The upper row shows a sequence of isodipole textures $T(1,\alpha)$ with decorrelations introduced by sporadic mutations. The lower row shows a sequence of isodipole textures $T(\alpha,1)$ with decorrelations introduced by propagated mutations. The parameter α is the degree of local correlation: $\alpha = 1$ for the fully structured "even" texture, $\alpha = 0$ for the random texture, and α has intermediate values for partially decorrelated textures.

Errors introduced by ϵ_{prop} are propagated through the texture, and thus destroy long-range correlations. Errors may also be introduced in a purely local ("sporadic") fashion. Let us denote the appearance of a check in row i and column j by $A_{i,j}$, where $A_{i,j} = +1$ denotes a bright check, and $A_{i,j} = -1$ denotes a dark check. Thus, the contrast of the check in row i and column j is equal to $A_{i,j}$ multiplied by an overall contrast value.

In the original even and odd textures, the appearance of all checks was faithfully determined by their states. That is, $A_{i,j} = a_{i,j}$. Sporadic errors may be introduced by nonfaithful rendition of the states $a_{i,j}$ into appearances $A_{i,j}$. The rate of nonfaithful rendition is indicated by ϵ_{spor}:

$$\text{prob}\{A_{i,j} = a_{i,j}\} = 1 - \epsilon_{spor}. \tag{3}$$

All of these textures are uncorrelated at orders 1, 2, and 3. This is the basic property that allows isolation of complex intracortical interactions (Victor, 1985, 1986). Higher-order correlations are most readily described by correlation parameters c_{prop} and c_{spor}. These quantities are related to the error rates by

$$c_{prop} = 1 - 2\epsilon_{prop} \tag{4}$$

and

$$c_{spor} = (1 - 2\epsilon_{spor})^4. \tag{5}$$

At order 4, the only nonzero correlations are those of the form

$$c_{I,J} = \langle A_{i,j} \cdot A_{i-I,j} \cdot A_{i,j-J} \cdot A_{i-I,j-J} \rangle, \tag{6}$$

where $\langle\ \rangle$ denotes an ensemble average over the texture. The value of this fourth-order correlation is (see Appendix 1):

$$c_{I,J} = c_{prop}^{|IJ|} c_{spor}, \qquad I, J > 0. \tag{7}$$

We will denote a texture constructed from error parameters ϵ_{prop} and ϵ_{spor} by $T(c_{prop}, c_{spor})$, where c_{prop} and c_{spor} are given by eqns. (4) and (5). In this notation, the texture $T(1,1)$ is the even texture, and $T(-1,1)$ is the odd texture of Julesz et al. (1978). Note that the textures $T(c_{prop},0)$ and $T(0,c_{spor})$ are statistically identical to the completely random texture $T(0,0)$ for any value of c_{prop} and c_{spor}.

For these experiments, we used two families of partially decorrelated textures: textures $T(1,\alpha)$ that have only sporadic decorrelation, and textures $T(\alpha,1)$ that have only propagated decorrelation. The above construction guarantees that for the same value of α, both kinds of textures have the same local correlation $c_{1,1} = \alpha$. However, these textures have very different long-range correlations. For I or J large, $c_{I,J}$ approaches zero for the propagated-decorrelation texture $T(\alpha,1)$, since $|\alpha|^{IJ}$ approaches zero as either I or J grow without bound. But for the sporadic-decorrelation texture $T(1,\alpha)$, $c_{I,J} = \alpha$ for all values of I and J.

These two extreme choices maximize the difference in long-range correlation but preserve equality of the short-range correlation $c_{1,1}$. Examples of the family of sporadic-decorrelation textures $T(1,\alpha)$ are shown in the top row of Fig. 1. Examples of the family of propagated-decorrelation textures $T(\alpha,1)$ are shown in the bottom row of Fig. 1. The textures $T(\alpha,1)$ and $T(1,\alpha)$, with $\alpha \leq 1$, will be referred to as "structured"; the texture $T(0,0)$ will be referred to as "random."

Measurement of visual evoked potentials

The stimuli described above were produced on a Tektronix 608 monitor (Beaverton, OR). Control signals for the raster display [horizontal (X), vertical (Y), and intensity (Z)] were generated by specialized electronics (Milkman et al., 1980) interfaced to an 11/73 computer. The display subtended 8.8 deg and had a luminance of 150 cd/m^2. Stimuli had a contrast $[(I_{max} - I_{min})/(I_{max} + I_{min})]$ of 0.4. The viewing distance was 57 cm except as otherwise noted.

Visual evoked potentials (VEPs) were elicited by periodic abrupt interchange between examples of two texture classes. In the first half of each stimulus cycle, an example of a particular texture T_1 was presented. In the second half of each stimulus cycle, an example of a second texture T_2 was presented. In each successive stimulus cycle, new examples of the texture classes T_1 and T_2 were displayed. Typically, T_1 was one of the structured textures $T(\alpha,1)$ or $T(1,\alpha)$, and T_2 was the random texture $T(0,0)$. Averaging was performed over the period that consisted of one presentation of each kind of stimulus. At each stimulus transition, each check of the texture had a probability of 50% of reversing contrast. There was no correlation between the positions of the checks that reversed in successive stimulus transitions. Thus, the averaged data included the summed response elicited by many examples of each stimulus. Each raw waveform represents an average of responses recorded in two or three 1-min runs. These runs were presented in randomized blocks.

Scalp signals were recorded differentially at C_z–0_z, P_z–0_z, C_z–0_1, C_z–0_2, amplified 10,000-fold, and bandpass-filtered (0.03–300 Hz) prior to digitization. Artifact rejection was performed by the computer prior to averaging. VEPs were saved by the 11/73 computer for off-line analysis that included Fourier analysis and modeling.

The subject pool for most experiments consisted of three normal volunteers, two male and one female; one of these subjects was naive to the purpose of the experiments. For one set of experiments, a fourth normal naive male was studied. Subjects ranged in age from 22–32 yr, and were corrected to normal visual acuity if necessary.

Results

The goal of these experiments is to arrive at a model for the neural interactions underlying processing of visual textures. The general approach, to be made quantitative in the Discussion, is to compare predictions of various models with experimental data. One class of simple models consists of linear processing, followed by a simple cortical nonlinearity such as rectification. These models predict how the responses to the basic even and odd textures will depend on check size. The first experiment will allow a test of these predictions.

Responses to the basic textures: dependence on check size

In this experiment, members of two texture classes were interchanged over a stimulus cycle of duration 473 ms (237 ms per texture). All six pairwise combinations of the three texture

classes {even, odd, random} were tested at check sizes ranging from 2.06–16.5 min.

In all conditions, responses at C_z–0_z were about 1.5 times as large as responses at P_z–0_z, and were similar in waveform. Responses at the lateral derivations C_z–0_1 and C_z–0_2 were nearly identical to those at C_z–0_z, and there were no consistent left/right asymmetries. These observations held in all other experiments described below, and we will focus on C_z–0_z from here on.

Typical averaged responses (at C_z–0_z) are shown in Fig. 2A. As in previous studies (Victor, 1986), these responses were decomposed into two components: a *symmetric* component, equal to the average of the responses following the two transitions of the stimulus cycle, and an *antisymmetric* component, equal to half of the difference of the responses to the two transitions of the stimulus cycle. The symmetric component is also equal to the sum of the *even* Fourier components of the original response, and the antisymmetric component is equal to the sum of the *odd* Fourier components of the original response. The symmetric component, which contains responses that are common to both transitions, is likely to be generated by activity at both cortical and precortical levels (Victor, 1986).

The symmetric components of the responses to texture interchange are shown in Fig. 2B. In all cases, there is a prominent occiput-positive transient (downward deflection) for all interchanges. This peak is analogous to the P-100, and likely contains potentials resulting from geniculate activity as well as cortical processing. The antisymmetric component (Fig. 2C), which contains only differential responses to the isodipole textures, does not contain a contribution from precortical processing (Victor, 1986); we focus on this component.

The antisymmetric component of the response to interchange of two independent sets of textures of the same class (even/even, odd/odd, or random/random) is essentially zero. This is experimental verification that the ensemble of textures is well-balanced for local luminance and contrast fluctuations. Antisymmetric-response components elicited by interchange between textures of distinct classes may be regarded as significantly different from zero if their size exceeds that of these responses elicited by interchange between statistically identical classes.

In all stimulus conditions involving interchange between distinct texture classes, antisymmetric components measured at all check sizes were indeed significantly different from zero by this criterion. At the smallest check size (2.06 min), the responses to even/random and odd/random interchange were similar, while the response to even/odd interchange was very small. At the larger check sizes, the odd/random response was smaller than the even/random response. The even/odd response was typically maximal at the intermediate check sizes (4.13 min and 8.25 min). To a first approximation, it appears that the even/odd response is approximately equal to the difference of the even/random response and the odd/random response; this will be examined below (see Fig. 7). As will be seen in the Discussion, this allows for some simplification of the modeling process.

Comparison of effects of sporadic and propagated decorrelation

One of the salient features of the basic even texture is the presence of contours that run its entire length (Fig. 1); this feature is absent from both the odd and the random textures. Another distinguishing feature of the even texture is the presence of rectangular blobs. Perhaps these features are important in the generation of the antisymmetric-response component.

This may be tested by examining the responses to interchange of the decorrelated textures $T(c_{\text{prop}}, c_{\text{spor}})$ and the random texture $T(0,0)$. The textures $T(1,\alpha)$ with only sporadic decorrelation have preserved long-range correlations; these textures have many long contours (top row of Fig. 1). The textures $T(\alpha,1)$ with only propagated decorrelation have long-range correlations that fall to zero [eqn. (7)]; long contours are much sparser than in $T(1,\alpha)$ for any value $0 < \alpha < 1$. The "long-contour" hypothesis predicts that an alteration of the even texture that destroys long-range correlation should abolish the antisymmetric response. Thus, interchange of $T(\alpha,1)$ (a texture with propagated decorrelations) with $T(0,0)$ should give no antisymmetric response component. This hypothesis also predicts that the antisymmetric response component elicited by interchange of $T(1,\alpha)$ (a texture with sporadic decorrelations) with $T(0,0)$ should be preserved.

The "blob" hypothesis has a very different prediction. In extreme form, it predicts that the antisymmetric-response component should be determined by the frequency of 2×2 rectangular blobs. Since the first three pixels of a 2×2 region are independent (second- and third-order correlations are zero), the frequency of such blobs depends only on the local fourth-order correlation $c_{1,1}$ [eqn. (6)]. However, this local correlation is exactly α [see eqn. (7) with $I = J = 1$]. Thus, if the antisymmetric response component depended only on the frequency of 2×2 blobs, then interchange of either $T(\alpha,1)$ or $T(1,\alpha)$ with $T(0,0)$ should yield equivalent responses.

The VEPs elicited by alternation between partially decorrelated textures and the random texture $T(0,0)$ are shown in Fig. 3. The "long-contour" hypothesis predicts that the antisymmetric response component is zero for textures $T(\alpha,1)$ with any propagated decorrelation (i.e. $\alpha < 1$). However, the antisymmetric response component is not zero, although it is less than the antisymmetric response component for the standard ($\alpha = 1$) texture. Values of α less than 1 result in an exponential decline in the frequency of contours of any given length, and no contours of indefinite length (Fig. 1). Thus, the observed dependence of responses to the propagated-decorrelation textures $T(\alpha,1)$ suggests that spatial interactions of an appropriately limited scale will account for the data.

On the other hand, antisymmetric responses are not identical for $T(\alpha,1)$ and $T(1,\alpha)$, contrary to the 2×2-blob hypothesis. Rather, responses elicited by textures with preservation of long-range structure [$T(1,\alpha)$] are larger than those elicited by textures without long-range structure [$T(\alpha,1)$], although preservation of long-range structure is not essential for the antisymmetric responses. This also suggests that neural interactions over some intermediate range, which covers regions larger than the 2×2-blobs but is not global, underlies the responses.

The above reasoning will be made quantitative in the Discussion. As a first step, we quantify the size of the antisymmetric component by the size of its first harmonic, as displayed in Fig. 4. For the textures with sporadic decorrelation, the size of the first harmonic is approximately proportional to the local correlation $c_{1,1} = \alpha$. For the textures with propagated decorrelation, the response is an accelerating function of the local correlation α. At low correlations, this response is less than the response to the textures with a sporadic decorrelation; at high

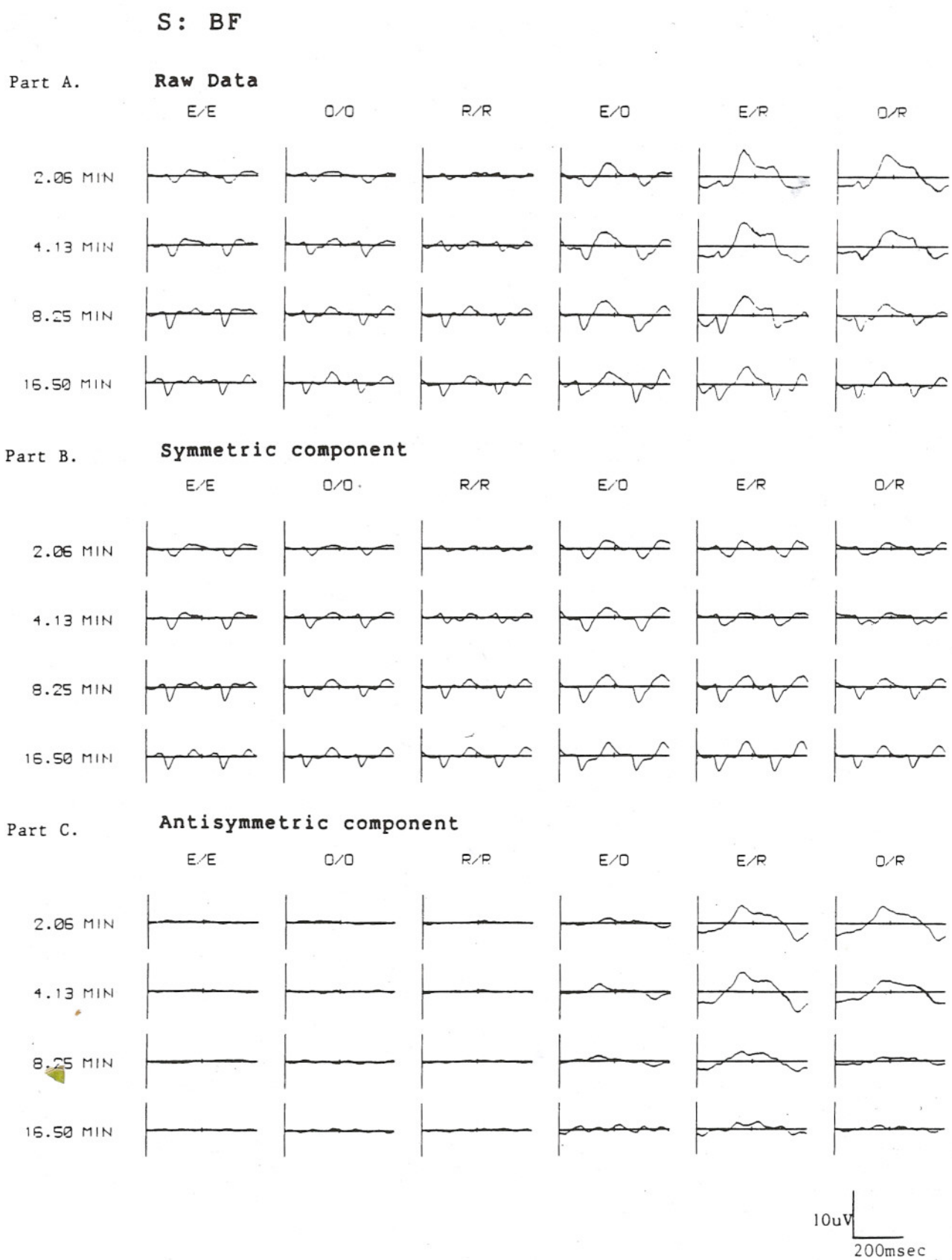

Fig. 2. Part A, averaged responses elicited by interchange between the basic even, odd, and random textures. Stimuli were at a contrast of 0.4 and the averaging period was 473 ms. Each averaged waveform is derived from two runs of one minute each. Part B, symmetric response components derived from the responses of Part A. Part C, antisymmetric response components derived from the responses of Part A. Subject: BF.

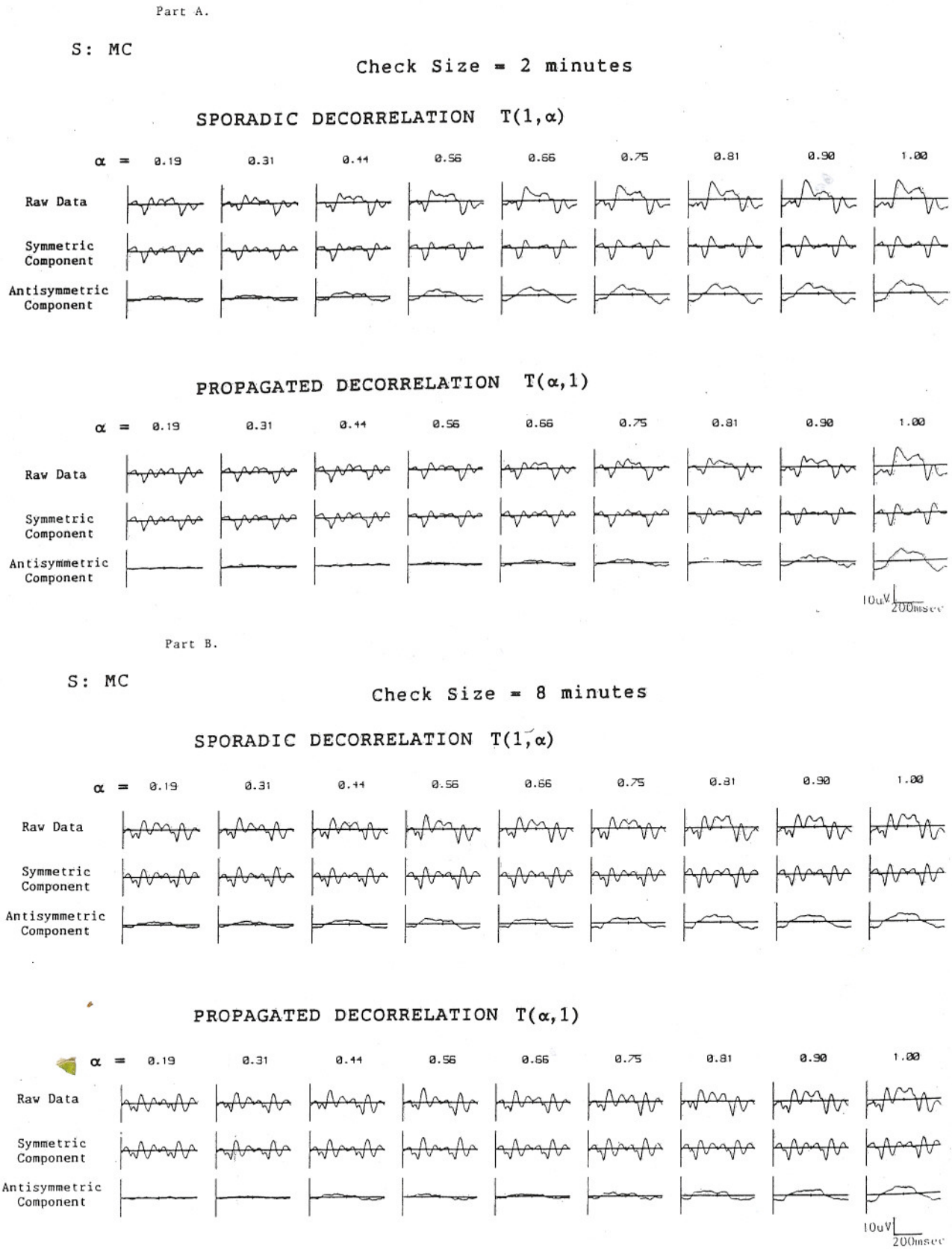

Fig. 3. Visual evoked responses elicited by interchange of partially decorrelated and random textures. In each panel, the averaged waveform is decomposed into a symmetric component (even harmonics) and an antisymmetric component (odd harmonics). The stimulus period was 473 ms. Part A, responses elicited by 2.06-min checks. Part B, responses elicited by 8.25-min checks. Subject: MC.

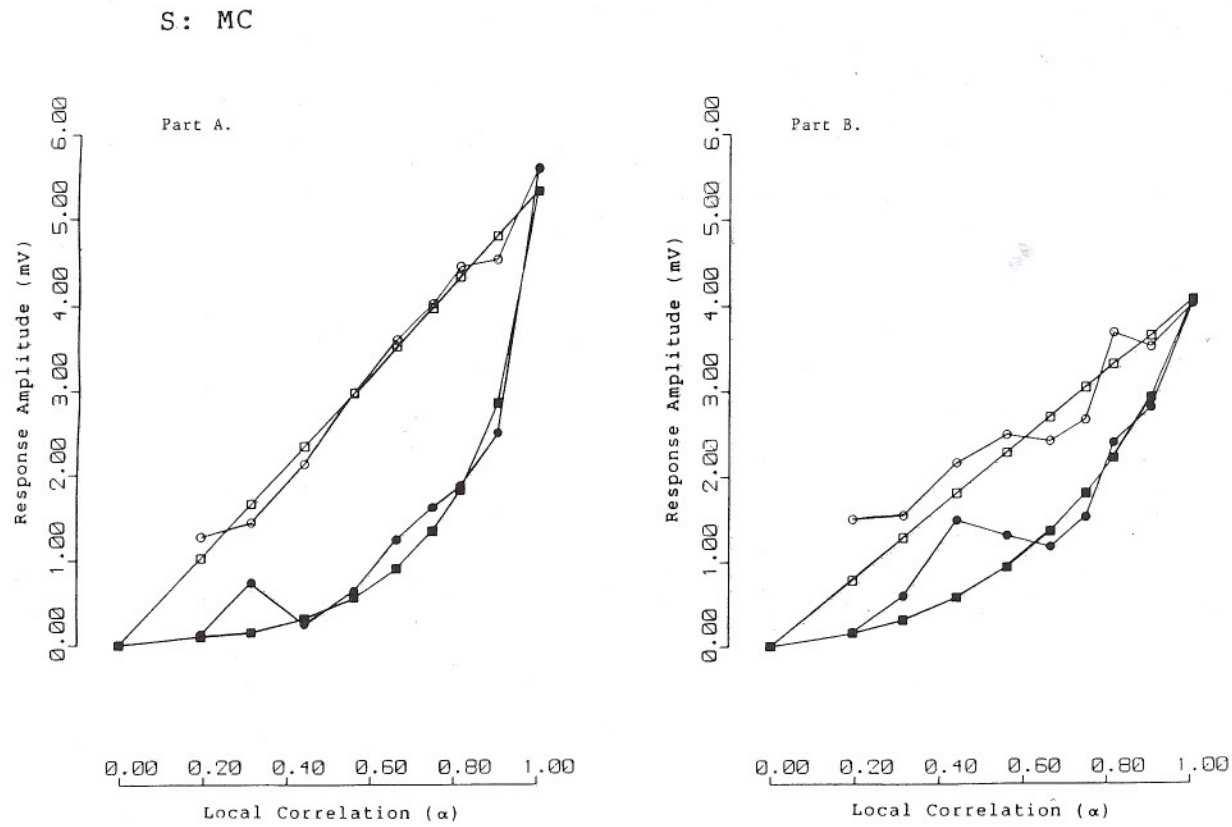

Fig. 4. The size of the antisymmetric response to structured/random texture alternation, as quantified by the amplitude of the first Fourier component of the response. Part A, responses elicited by 2.06-min checks. Part B, responses elicited by 8.25-min checks. Data (circles) are from Fig. 3. Open symbols: sporadic decorrelation; filled symbols: propagated decorrelation. Fits to the data (squares) are calculated from the model described in the Discussion. The one-dimensional exponential weighting $w(x,y) = (1/2D)e^{-|x|/D}\delta(y)$ is used.

correlations, the responses to the two texture classes are similar. The form of this dependence will allow specific hypotheses for the spatial scale of nonlinear interactions to be tested.

Dependence of response dynamics on strength of correlation

The waveforms of the antisymmetric components, as shown in Fig. 3, appear to vary in amplitude but not in shape as correlation structure is varied. Thus, to a first approximation, the data of Fig. 3 suggest that the dynamics of the cortical response are independent of the spatial extent of the correlation structure. However, since these responses were measured at a relatively slow interchange rate, subtle changes in dynamics might not be apparent.

Figure 5 examines the response dynamics in more detail. Antisymmetric response components were extracted from the VEP elicited by interchange of partially decorrelated and random textures, at a range of stimulus repetition rates: 2.11 Hz (473 ms period, 237 ms per texture) to 16.9 Hz (59 ms period, 30 ms per texture). The dependence of amplitude and phase of the fundamental response on both temporal frequency and local correlation is plotted as color-coded contour map: response amplitude is represented by the height of the contour map, and response phase is represented by the color of the contour lines.

For any fixed value of correlation α, the antisymmetric-response size decreased with increasing frequency over the entire repetition rate tested. As temporal frequency increases, the response has increasing phase lag. Responses at reversal rates above 10 Hz were not distinguishable from noise.

The hypothesis that response dynamics are independent of the degree of correlation structure has two implications: one for response amplitude, and one for response phase. If dynamics and degree of correlation are independent, then the amplitude of the response should be a product of two terms: one dependent only on the reversal rate, and one dependent only on the degree of correlation. This in turn implies that contour lines should run approximately parallel to either the temporal-frequency axis, or the local-correlation axis, and should have squared-off "corners" at the high-temporal-frequency, low-correlation (upper left) region of each contour map. As seen from Fig. 5, this prediction is supported by the data.

The hypothesis that response dynamics are independent of the degree of correlation implies that the phase lag is independent of the degree of decorrelation. In particular, regions of constant color (which indicate responses of constant phase) should run parallel to the horizontal axis (degree of correlation). As seen from Fig. 5, this prediction is also approximately true. There is a slight tendency for these regions of constant color to slant toward higher temporal frequencies at lower degrees of local correlation. This slant corresponds to a phase shift of at most 0.125π radians, or one-sixteenth of a cycle.

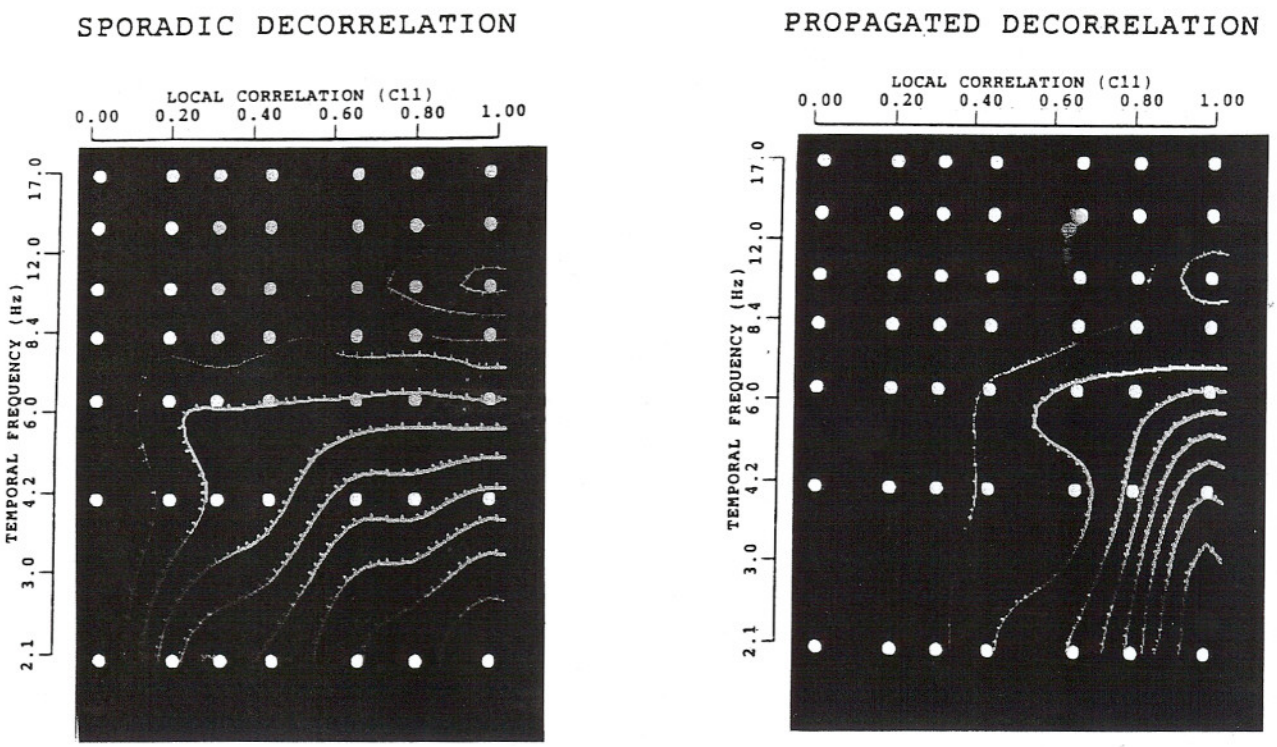

Fig. 5. Amplitudes and phases of the fundamental component of the response elicited by interchange of partially decorrelated and random textures, as a function of stimulus period and degree of local correlation $c_{1,1} = \alpha$. Check size: 8.25 min. Part A, interchange of sporadic-decorrelation textures $T(1,\alpha)$ with the random texture. Part B, interchange of propagated-decorrelation textures $T(\alpha,1)$ with the random texture. Amplitude and phase of the fundamental response are plotted as a color-coded contour map. Amplitude is represented by the height of the contour map; each contour line represents 0.5 μV and the tickmarks point downhill. Phase of the fundamental component is represented by the color of the contour lines, with green indicating a phase of zero, red indicating a phase shift of one-half a cycle, blue a phase lag of one-quarter cycle, and yellow a phase lead of one-quarter cycle. Thus, real-valued quantities appear with a color along the red–green line, and imaginary-valued quantities appear with a color along the blue–yellow line. Subject: JV.

Another feature of the frequency response of the antisymmetric response is that above 10 Hz, (50 ms per texture), the antisymmetric component is nearly absent. However, VEP components driven by the checkerboard-pattern appearance persist at these higher temporal frequencies (Victor & Conte, 1987*a*). There are two ways in which the difference in dynamics between the antisymmetric VEP generated by isodipole patterns and that generated by pattern appearance might arise: (1) This difference in dynamics might reflect differences at the level of the retinal input to the highly nonlinear pattern-processing mechanism. (2) Alternatively, there may be additional sluggish dynamics at or after a stage of the cortical nonlinearity which generates the antisymmetric isodipole VEP.

A further stimulus manipulation provides clear evidence that this temporal filtering occurs late in processing. We use a stimulus period of 947 ms, corresponding to a stimulus rate (fundamental) of 1.06 Hz. However, each half of the stimulus period (473 ms) contains not one texture but a sequence of N examples of each texture class ($N = 1, 2, 4, 8, 16, 32$) presented sequentially. (Thus, for $N = 16$, each texture is presented for 473 ms/16 = 30 ms.) This stimulus elicits a VEP timed to each new stimulus presentation; superimposed on this, a response to texture *class* is apparent (Fig. 6A). This response may be extracted by Fourier analysis at the fundamental frequency of 1.06 Hz (Fig. 6B).

If the temporal integration responsible for attenuation of the responses at high temporal frequencies were prior to the stage at which the high-order correlation structure of the even stimulus was processed, this manipulation would abolish the antisymmetric-response component. Instead (Fig. 6B), even when each individual texture example is presented for 15 ms, the antisymmetric response is present; at presentations of 30 ms, the antisymmetric response has attained two-thirds of its full size. Thus, the sluggish dynamics revealed by Fig. 5 cannot occur prior to processing the correlation structure of the textures.

Discussion

Implications for models of cortical processing

Our plan is to use the experimental results described above to deduce some properties of the cortical processing of complex

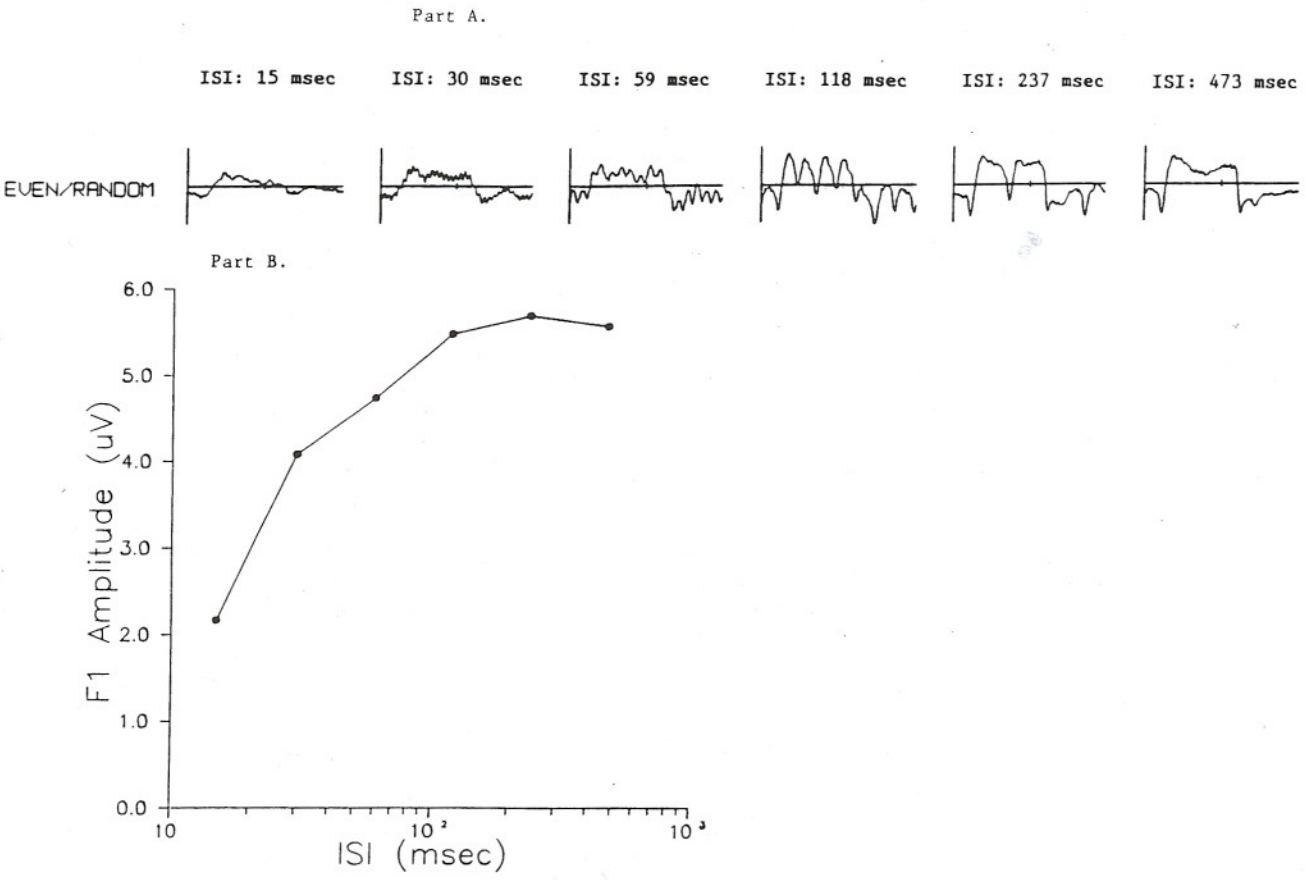

Fig. 6. Part A, responses to interchange of even and random textures, with presentations of multiple examples of each texture within the 473-ms period allotted for each texture class. Check size: 4.13 min. Part B, size of the fundamental Fourier component of the responses of Part A. Subject: JV.

patterns. We will heavily exploit the statistical properties of the basic even and odd textures. These statistical properties guarantee that linear and simple nonlinear mechanisms do not contribute to an antisymmetric response component. Thus, we previously hypothesized that the antisymmetric response component was not generated by differences between population activity at subcortical levels either directly or as expressed in synaptic potentials of retinocortical afferents; rather, the antisymmetric response component reflected and required cortical processing (Victor, 1985; Victor & Zemon, 1985). This conclusion was based on the inability of known retinal mechanisms (linear summation and rectification) to generate the required neural signals. It was supported by experimental studies in the anesthetized cat: analogous isodipole stimuli elicited an antisymmetric cortical VEP component, while simultaneous monitoring of population activity at the geniculate level contained no antisymmetric component (Victor, 1986).

The statistical equivalences between the basic even and odd textures are shared by all of the textures used in the present study. These are (1) identical average luminance, (2) identical second-order (pairwise) autocorrelation (and therefore identical power spectra), and (3) identical third-order correlation statistics. These equivalences were demonstrated for single examples of the textures that are infinite in spatial extent (Julesz et al., 1978). However, the equivalences also hold for averages over a large number of independent finite examples of the textures—the experimental paradigm used.

Because of these statistical properties, it follows that neural mechanisms that generate the antisymmetric response must contain nonlinearities whose formal order is at least four, and which involve nonlinear interactions among at least four checks of the texture. We consider a general model framework in which the output of local linear mechanisms (center/surround) and simple nonlinear mechanisms (subunits) are the input to a more complex cortical process, whose spatial range and dynamics are at present unspecified. The form of the initial stages of the model are motivated by retinal and geniculate physiology (Enroth-Cugell & Robson, 1966, Hochstein & Shapley, 1976, de Monasterio, 1978, Kaplan & Shapley, 1982). However, our arguments depend only on the hypotheses that these initial stages consist either of linear processes or rectifying subunits. Thus, these stages represent not only retinal and geniculate processes, but also the early stages of cortical processing (Movshon et al., 1978*a*, *b*, Spitzer & Hochstein, 1985*a*, *b*).

Analytic treatment of a prototypical example

We proceed to refine this model framework on the basis of the experimental data described above. Consider first a cortical

nonlinearity that sums inputs over a particular $m \times n$ rectangular region and then applies a nonlinear function. The input–output relationship for the nonlinear function is taken to be a fourth-power law

$$r(t) = [s(t)]^4, \tag{8}$$

where $s(t)$ is the summed input to the nonlinearity and $r(t)$ is the output of the nonlinearity. Although this summation profile and the nonlinearity (8) are rather unphysiologic, they provide for a direct analytic treatment. The analysis also extends in an approximate fashion to more physiologic models.

The average response of the fourth-power nonlinearity (8) to an $m \times n$ rectangle is calculated in Appendix 2. We now compare these results [eqns. (35), (38), and (42)] to the observed responses to interchange of the random, even, and odd textures. One important limiting case is that of large m and n. This corresponds to a large number of checks in each rectangular summing region. In this limit, we find $M_{\text{even}} = 9m^2n^2$, $M_{\text{odd}} = 6m^2n^2$, $M_{\text{ran}} = 3m^2n^2$; the ratio of the fourth moments M_{even}:M_{odd}:M_{ran} is 3:2:1. The model prediction, then, is that for small check sizes, the response to even/random interchange should be the largest, and should be approximately twice the size of both the response to even/odd and odd/random interchange. However, at small check sizes, the response to even/random interchange is approximately equal to the response to odd/random interchange; the response to even/odd interchange is close to zero (Fig. 2C).

A second important limiting case is that of long but narrow summing regions (i.e. m large but $n = 2$). In this limit, we find $M_{\text{even}} = 24m^2$, $M_{\text{odd}} = 12m^2$, $M_{\text{ran}} = 12m^2$; the ratio of the fourth moments M_{even}:M_{odd}:M_{ran} is 2:1:1. At small check sizes, this predicts that the even/odd and even/random responses should be comparable, and that the odd/random response is negligible. This also is contrary to the data (Fig. 2C).

A third limiting case is $m = n = 2$. This situation was analyzed in detail previously (Victor, 1985), and was excluded because it could not generate an antisymmetric response component comparable in size to the symmetric response component.

Extension to more "physiologic" models

Thus, we have seen that the $m \times n$-summing region, coupled with a fourth-power nonlinearity, cannot lead to the behavior observed experimentally. As we now show, the analysis extends to models with more physiologically reasonable patterns of spatial summation and to more general static nonlinearities. Thus, the basic conclusion extends to these models as well.

Extension to other patterns of spatial summation is a consequence of spatial symmetries of the textures. Consider, for example, a mechanism that has excitatory input from one row of checks $(0,0)$–$(0, n-1)$, and equally potent inhibitory input from a flanking row of checks $(1,0)$–$(1, n-1)$. That is, the input to the nonlinearity is the algebraic difference of the intensity summed over the first row and the intensity summed over the second row. This mechanism will produce the same average response (averaged over an ensemble of textures) as would a mechanism that summed excitatory input (only) over the $2 \times n$ rectangle made up of the two rows. This is because inversion of the state of one row of checks always produces another example of the same texture class. Inversion of one row of checks corresponds to changing the state of one check $a_{1,0}$ in the first column used to generate the textures; this merely selects another example out of the same ensemble because states are assigned to the first row and column in an unbiased and independent manner.

Spatial profiles consisting of concentric rectangular regions of excitation and inhibition can be analyzed in a fashion strictly analogous to the analysis given above for the odd texture: the expression for the fourth moment does not factor, but does break up into manageable terms analogous to the decomposition given by eqn. (40).

Physiologically realistic spatial profiles that are not evenly weighted and do not line up in register with the check borders will produce responses that do not correspond precisely with those of uniform rectangular regions. The effects of spatial structure are likely to have the greatest impact when the spatial regions are in register with the lattice, and have comparable spatial weighting. Numerical calculations based on some examples of out-of-register profiles (e.g. diagonal strips and circles) indicate that such models do have qualitatively similar behavior.

The lack of suitability of the above model also extends to other nonlinearities. In any given operating range, a nonlinear transformation $r(t) = f[s(t)]$ (such as saturation, threshold, or rectification) can be approximated by an expression of the form

$$f[s(t)] \simeq b_0 + b_1 s(t) + b_2[s(t)]^2 + b_3[s(t)]^3 + b_4[s(t)]^4, \tag{9}$$

where the coefficients b_i are derived from either Taylor expansion or orthogonal functional expansion of the nonlinearity f. For example, orthogonal expansion of a power-law rectified nonlinearity

$$r(t) = |s(t)|^\gamma, \tag{10}$$

in terms of Hermite polynomials yields a coefficient b_4 that is less than zero for powers $\gamma < 2$ and greater than zero for powers $\gamma > 2$ (Victor, 1988). Whatever the nature of the nonlinearity f, the statistical equivalences of the textures imply that the terms b_0, b_1, b_2, and b_3 cannot generate an antisymmetric response component; thus, to a first approximation, only the b_4 term [which corresponds to eqn. (8)] matters. Additional symmetry constraints imply that only even-order terms can contribute; thus, the next significant term is $b_6[r(t)]^6$.

In sum, the above analysis excludes models based on linear summation followed by a single static nonlinearity. Although sufficiently high-order nonlinearities may produce *some* antisymmetric-response components, the qualitative dependence of this response on the texture type and check size does not conform to the data. Furthermore, numerical studies of the nonlinearity (10) indicate that this model does not account for the relative size of the symmetric and antisymmetric VEP components (Victor 1985, Fig. 7).

Models not excluded

The above analysis does *not* exclude models other than those within the linear summation/pointwise nonlinearity framework. For example, a multiplicative interaction between four texture regions will discriminate even, random, and odd textures, be-

cause of the key fourth-order correlation (2). Although multiplication of four local signals representing signed contrast would seem quite unphysiologic, an equivalent computation can be readily generated out of familiar elements.

High-order nonlinear transformation of a signal generated by summing a region that includes at least four checks of the texture would in principle also contain a quadruple product. This is essentially because $(w+x+y+z)^4$ contains the term $24wxyz$ in its multinomial expansion. The size of this cross-term is small in comparison to the size of terms that do not involve interactions of all four inputs, such as w^2xy, w^2x^2, w^3x, and w^4. Thus, the relative size of the antisymmetric VEP is not explained by this kind of model. However, a simple power law, saturation, or threshold might generate the requisite interactions, provided that additional parallel nonlinearities act to cancel the terms involving fewer than four distinct inputs.

A second, perhaps more plausible, construct depends on serial nonlinearities, rather than cancellation. Edge detection (independent of edge polarity) is clearly a nonlinear process and is tantamount to a local pairwise multiplication (Emerson et al., 1987), or rectification (Spitzer & Hochstein, 1985*a*, *b*) of an odd-symmetric line-weighting profile. A subsequent pairwise nonlinear operation on two signals generated by such mechanisms would thus effectively result in a product of four local contrast signals.

Determination of the spatial scale of nonlinear interactions

Although we are unable to specify a precise model for the local nonlinear interactions, we are still able to ascertain the spatial scale and approximate spatial-weighting function for the combination of nonlinear signals. This analysis rests on the dependence of the antisymmetric-response component on the correlation structure of the textures (Fig. 4).

One major feature of the data is that for high degrees of local correlation and large check sizes, the antisymmetric VEP response size is relatively insensitive to the presence or absence of long-range correlation (Fig. 4B). However, as the degree of local correlation decreases, textures with long-range correlation produce larger VEPs than do textures without long-range correlation. A similar effect of correlation structure on texture discriminability was observed in psychophysical experiments (Victor & Conte, 1987*b*). The antisymmetric VEP component is an electrophysiological correlate of differential activity of neural populations driven by structured and random textures. The correspondence of the VEP data and psychophysics is reassuring in that it demonstrates that some of this differential neural activity is accessible to later stages of visual processing. However, no direct causal relationship between the VEP and the psychophysical response is implied.

If the processes that generated psychophysical discrimination and the antisymmetric VEP component were purely local, then both measures would depend solely on the local correlation $\alpha = c_{1,1}$. Conversely, if these processes depended on very long-range correlations, then even slight local decorrelation, if propagated, would destroy both psychophysical distinguishability and the antisymmetric VEP response. The data fall between these two extremes. This suggests that the relevant interactions have a range that is larger than an individual check of the stimulus, but is not indefinitely large.

This notion can be made more quantitative with the aid of a model. To account for the observed behavior, we postulate that local linear and nonlinear processes are combined by a second nonlinear stage. This second nonlinear stage has a spatial weighting, denoted $w(x,y)$, which is neither pointlike nor concentrated at large distances. The spatial weighting is assumed to be normalized by $\iint w(x,y)\mathrm{d}x\mathrm{d}y = 1$.

Let $c(x,y)$ be the fourth-order correlation between points at locations (0,0), $(x,0)$, $(0,y)$, and (x,y) of a test stimulus. These coordinates (x,y) are physical units, not measured in units of check size. Therefore (choosing the center (0,0) to coincide with a corner of a check),

$$c(x,y) = c_{1+\lfloor |x|/h \rfloor, 1+\lfloor |y|/h \rfloor}, \tag{11}$$

where h denotes the size of each check.

We postulate that the response $R(c_{\mathrm{prop}}, c_{\mathrm{spor}}, h)$ to the texture $T(c_{\mathrm{prop}}, c_{\mathrm{spor}})$ constructed on a lattice of check size h is a function of the correlations $c(x,y)$ as weighted by the spatial weighting of the nonlinearity $w(x,y)$. That is,

$$\begin{aligned} R(c_{\mathrm{prop}}, c_{\mathrm{spor}}, h) &= f\left(\iint c(x,y)\,w(x,y)\mathrm{d}x\mathrm{d}y\right), \\ &= f\left(\iint c_{\mathrm{prop}}^{(1+\lfloor |x|/h \rfloor)(1+\lfloor |y|/h \rfloor)} c_{\mathrm{spor}}\, w(x,y)\mathrm{d}x\mathrm{d}y\right), \end{aligned} \tag{12}$$

where the last step follows by using the eqns. (7) and (11) for $c(x,y)$. (In this derivation, we neglect effects related solely to the discrete nature of the lattice.)

The experimental data permit a crucial simplification. Empirically (Fig. 4), the responses to the sporadic-decorrelation textures $T(1,\alpha)$ have amplitudes that are very nearly proportional to the local correlation α. This proportionality constant will be denoted $K(h)$, to highlight its dependence on the check size h:

$$R(1,\alpha,h) = K(h)\alpha. \tag{13}$$

For the textures $T(1,\alpha)$ with sporadic decorrelation only, the model prediction obtained from (12) with $c_{\mathrm{prop}} = 1$ is

$$\begin{aligned} R(1,\alpha,h) &= f\left(\iint \alpha w(x,y)\mathrm{d}x\mathrm{d}y\right), \\ &= f(\alpha), \end{aligned} \tag{14}$$

since $w(x,y)$ is assumed to be normalized. Combining eqns. (13) and (14) results in a relation for the unknown function f:

$$f(\alpha) = K(h)\alpha. \tag{15}$$

This proportionality constant $K(h)$ was fit to measure responses to the texture $T(1,\alpha)$ by a linear least-squares procedure. $K(h)$ is thus approximately equal to the antisymmetric response to alternation between an even texture $[T(1,1)]$ and a random texture.

Next, eqns. (15) and (12) may be combined to provide a prediction of the responses to the propagated-decorrelation textures $T(\alpha,1)$:

$$R(\alpha,1,h) = K(h)\iint \alpha^{(1+\lfloor |x|/h \rfloor)(1+\lfloor |y|/h \rfloor)} w(x,y)\mathrm{d}x\mathrm{d}y. \tag{16}$$

Correspondence of model and data: determination of spatial scale

Several choices for the weighting function $w(x,y)$ were evaluated empirically for their ability to explain [through eqn. (16)] the observed dependence of the response $R(\alpha,1,h)$ on α. These test functions included one- and two-dimensional Gaussians, one- and two-dimensional exponential distributions, distributions that were concentrated at a fixed distance, and distributions that were uniform within a given radius but zero outside of this radius. These trial functional forms, with spatial scales free to vary, were substituted for $w(x,y)$ in eqn. (16). For example, the one-dimensional weighting used was

$$w(x,y) = (1/2D(h))e^{-|x|/D(h)}\delta(y), \tag{17}$$

where the parameter $D(h)$ represents the overall spatial scale of the nonlinear interaction. Substitution of eqn. (17) into eqn. (16) yields

$$R(\alpha,1,h) = \frac{\alpha K(h)}{1 - \frac{D(h)\ln\alpha}{h}}. \tag{18}$$

The spatial scale $D(h)$ was determined by minimizing the squares of the differences between the prediction (18) and the observed responses to interchange of the textures $T(\alpha,1)$ with the random texture. The fit provided by eqn. (18) is illustrated by the smooth curves and square symbols in Fig. 4, with values $D(h) = 13.9$ for check size $h = 2.06$ min, and $D(h) = 20.4$ for check size $h = 8.25$ min.

In all four subjects, the exponential weighting functions provided fits that were superior to the fits provided by the other distributions. However, there was no consistent trend in favor of either the one-dimensional or the two-dimensional weighting function.

A model prediction: little temporal context dependence

This model, of simple linear and local nonlinear processes that are combined by a second nonlinearity, makes other specific predictions. Implicit in the construction of the model is the notion that the response to a particular texture is independent of the temporal "context" of the texture. As shown in Appendix 3, this leads to the prediction [eqn. (45)] that the antisymmetric component elicited by even/odd interchange should be equal to the algebraic difference of the antisymmetric components elicited by even/random and odd/random interchanges. This is tested in Fig. 7. There is reasonable agreement with experimental data.

A model prediction: little coupling of dynamics to correlation structure

The preceding analysis [eqn. (16)] predicts that the responses to interchange of structured and random isodipole textures all share a common phase. The prediction is approximately true (Fig. 3); phase shifts due to changes in correlation structure were no more than 0.125π radians (Fig. 5). This is evidence in favor of a basically static nonlinearity, since dynamics depend only slightly on correlation structure. The ability of the model to account for the dependence of response amplitude on the spatial extent of correlation supports the interpretation of this dependence in terms of simple spatial exponential weighting, rather than in terms of model dynamics.

Variation of scale of interaction with check size

The analysis above was applied to data from all subjects at check sizes ranging from $h = 1.06$ min to 16.5 min. The spatial scale $D(h)$ determined by least-squares fitting of eqn. (18) to observed responses is shown in Fig. 8. (To obtain data for a check size of 1.03 min, the standard viewing distance was doubled to 114 cm.) For small checks (1.03–4.13 min), the deduced interaction length D is approximately 10–15 min. This is somewhat larger than the 8-min aperture that Gagalowitz (1981) and Gagalowitz and Ma (1985) used to account for certain aspects of complex texture perception.

The interaction length deduced from responses to larger check sizes (4.13–16.5 min) grows proportionally with the size of the check. One possible reason is that cortical interaction length simply scales along with other size parameters of retinal and cortical function organization (Levi et al., 1985). Thus, proportionality of apparent interaction length and check size would be expected if the larger-check patterns elicited responses primarily from more eccentric locations. In this interpretation, the similarity of the interaction length $D(h)$ at the smaller check sizes is a consequence of the more nearly constant cortical magnification factor within the fovea (Dow et al., 1984).

This possibility was tested by experiments in which the isodipole stimulus was restricted to 1-deg-wide annuli. The masked portion of the visual field was maintained at the mean luminance. The amplitudes of the antisymmetric response to even/random interchange for two subjects are shown in Fig. 9. In both cases, there is a substantial dependence of response on eccentricity. However, the rank order of response sizes (2 min checks > 4, 8, min checks > 16 min checks) is basically independent of eccentricity. Although absolute response is highly dependent on eccentricity, regions of all eccentricities tested contributed in approximately the same proportion to small-check responses as they did to large-check responses. The hypothesis that the small-check responses are exclusively due to foveal input and the large-check responses are due to more peripheral input is not supported.

The VEP signals evoked by these masked stimuli are small, and small differences in the weighting of inputs from different eccentricities could be missed. However, the data of Fig. 9 make it unlikely that the change in interaction length $D(h)$ with check size is solely due to differential stimulation of cortical areas by the different check sizes. An alternative possibility is that, at each cortical location, processing takes place at a range of spatial scales. At any given cortical location, it is known that units covering more than a ten-fold range of spatial-frequency selectivities exist (De Valois et al., 1982); the evidence presented here suggests that this heterogeneity in the spatial scale of linear processes is accompanied by a similar heterogeneity in the scale of intracortical nonlinear interactions.

Appendix 1: The correlation statistics of the generalized even and odd textures

Here we demonstrate that the generalized even and odd textures are statistically homogeneous, that their second- and third-

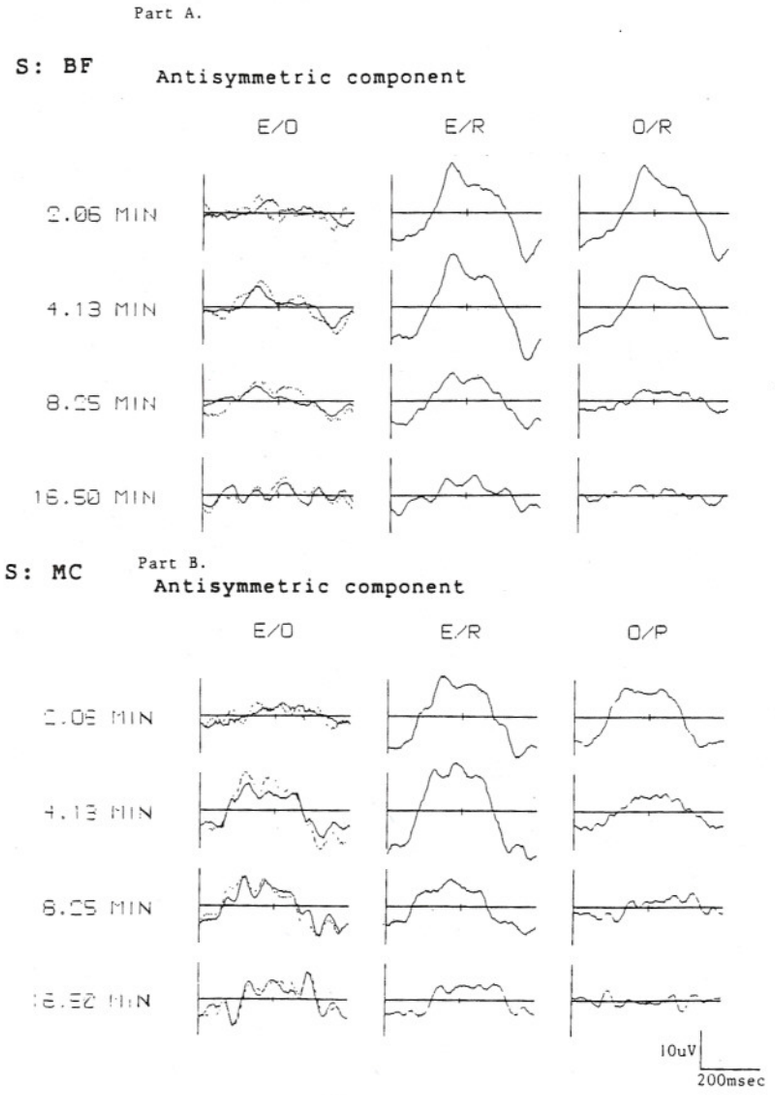

Fig. 7. A test of the hypothesis that responses are independent of temporal context, for four check sizes and two subjects. This hypothesis predicts that the antisymmetric component of the response to even/odd interchange (solid line, first column) is the difference of the antisymmetric components to even/random (second column) and to odd/random (third column) interchange. This difference is plotted as the broken line in the first column. Subjects: BF (Part A) and MC (Part B). Data from subject BF is taken from Fig. 2.

order correlation statistics are zero, and verify that the only nonzero fourth-order correlation statistics are given by

$$c_{I,J} = c_{\text{prop}}{}^{|IJ|} c_{\text{spor}}, \qquad I, J > 0. \tag{19}$$

This is essentially a generalization of Theorems I and IV of the Appendix of Victor (1985), which considered only $c_{\text{prop}} = \pm 1$ and $c_{\text{spor}} = 1$.

To see that the second- and third-order correlations are zero, it suffices to observe that checks that lie in either a different row or a different column are independent. This follows from the fact that reversing the state of a single check $a_{0,j}$ in the initial row of a texture results in another texture of the same class. This alteration reverses the states of all of the checks in column j. Thus, the state of a single check in an arbitrary column j is independent of the state of all other checks in distinct columns, since this is equally likely to be $+1$ or -1 depending only on the choice of $a_{0,j}$. A similar argument holds for the rows. Thus, correlations among a cluster of checks can only be nonzero if each row or column that contains any check contains at least two checks. (A slightly more detailed argument shows that each row or column must contain an *even* number of checks.) The simplest way that this can occur is if the cluster contains four checks, two each in two rows and columns.

The argument just given indicates that all of the checks in any given row are independent, as are all of the checks in any given column. Thus, any row and any column could have been chosen as the initial row and column. This means that the textures are homogeneous in a statistical sense: local features are equally likely to occur anywhere in the texture; the choice of

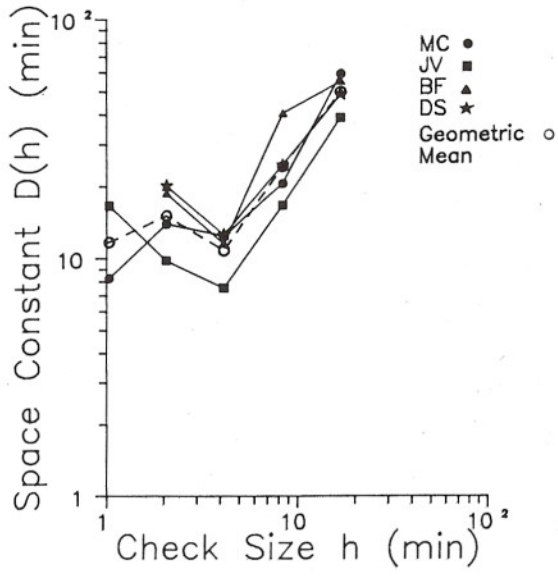

Fig. 8. Apparent space constant $D(h)$ as a function of check size h for four subjects.

index row and column is irrelevant. Another important consequence of this is that spatial averages over a particular texture example may be replaced by averages in a finite spatial region sampled over the entire texture ensemble (ergodicity).

The proof of eqn. (19) may be broken into two parts: one that handles $c_{\text{prop}} \neq 1$, and one that handles $c_{\text{spor}} \neq 1$. To do this, we first observe that any texture $T(c_{\text{prop}},c_{\text{spor}})$ can be written as a product of two textures $T(c_{\text{prop}},1)$ and $T(1,c_{\text{spor}})$; under this factorization, the correlation structure factors as well. More generally, if the states $a'_{i,j}$ and labelings $A'_{i,j}$ belong to $T(c'_{\text{prop}},c'_{\text{spor}})$, and the states $a''_{i,j}$ and labelings $A''_{i,j}$ belong to $T(c''_{\text{prop}},c''_{\text{spor}})$, we will show that the states $a_{i,j} = a'_{i,j}a''_{i,j}$ and labelings $A_{i,j} = A'_{i,j}A''_{i,j}$ belong to the texture $T(c_{\text{prop}},c_{\text{spor}})$ with

$$c_{\text{prop}} = c'_{\text{prop}}\,c''_{\text{prop}} \tag{20}$$

and

$$c_{\text{spor}} = c'_{\text{spor}}\,c''_{\text{spor}}. \tag{21}$$

This factorization is generic for plane Markov process textures, and is independent of the particular recursion relation used.

To deduce eqn. (20), observe that in the product texture, the relation $a_{i,j}\cdot a_{i-1,j}\cdot a_{i,j-1}\cdot a_{i-1,j-1} = 1$ holds if either the analogous relationship holds for both factor textures $T(c'_{\text{prop}},c'_{\text{spor}})$ and $T(c''_{\text{prop}},c''_{\text{spor}})$, or for neither factor texture. Thus, according to eqn. (2),

$$1 - \epsilon_{\text{prop}} = (1 - \epsilon'_{\text{prop}})(1 - \epsilon''_{\text{prop}}) + \epsilon'_{\text{prop}}\epsilon''_{\text{prop}}, \tag{22}$$

from which it follows that

$$1 - 2\epsilon_{\text{prop}} = (1 - 2\epsilon'_{\text{prop}})(1 - 2\epsilon''_{\text{prop}}). \tag{23}$$

The relation (20) follows from the definition (4) of c_{prop}.

To deduce eqn. (21), observe that $a_{i,j}$ is faithfully rendered as $A_{i,j}$ if either both $a'_{i,j}$ and $a''_{i,j}$ are faithfully rendered, or neither are faithfully rendered. Thus, according to eqn. (3),

$$1 - \epsilon_{\text{spor}} = (1 - \epsilon'_{\text{spor}})(1 - \epsilon''_{\text{spor}}) + \epsilon'_{\text{spor}}\epsilon''_{\text{spor}}, \tag{24}$$

from which it follows that

$$1 - 2\epsilon_{\text{spor}} = (1 - 2\epsilon'_{\text{spor}})(1 - 2\epsilon''_{\text{spor}}). \tag{25}$$

The relation (21) follows from the definition (5) of c_{spor}.

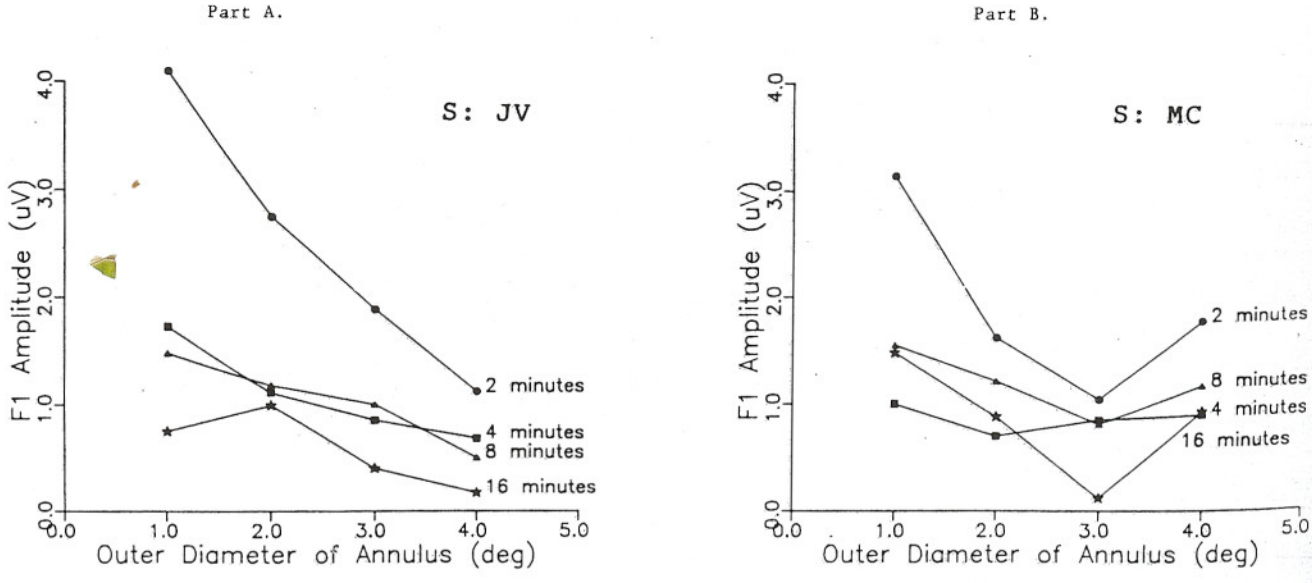

Fig. 9. Dependence of the amplitude of the fundamental Fourier component of the response to even/random interchange on eccentricity. The basic even and random stimuli were masked by a 1-deg circular annulus whose outer diameter is indicated on the abscissa. Contrast: 0.4. Stimulus period: 473 ms. Subjects: JV (Part A) and MC (Part B).

Now we consider separately the correlation structure of the textures $T(c_{\text{prop}},1)$ and $T(1,c_{\text{spor}})$.

The sporadic-decorrelation textures $T(1,c_{\text{spor}})$ are easier to handle. These textures have a deterministic underlying state assignment $a_{i,j}$ that obeys

$$a_{i,j}\cdot a_{i-I,j}\cdot a_{i,j-J}\cdot a_{i-I,j-J}=1 \tag{26}$$

[Theorem I of Victor (1985)]. Rendering of the states $\{a_{i,j},a_{i-I,j},a_{i,j-J},a_{i-I,j-J}\}$ into appearances $\{A_{i,j},A_{i-I,j},A_{i,j-J},A_{i-I,j-J}\}$ results in a collection of appearances whose product is 1 if an even number ($n=0$, 2, or 4) of states were rendered nonfaithfully; if an odd number of states are rendered nonfaithfully ($n=1$ or 3), the product of the appearances is -1. Faithful rendition occurs with probability $1-\epsilon_{\text{spor}}$. Thus,

$$\begin{aligned} c_{I,J} &= \langle A_{i,j}\cdot A_{i-I,j}\cdot A_{i,j-J}\cdot A_{i-I,j-J}\rangle, \\ &= \sum_{n=0}^{4}(-1)^n(1-\epsilon_{\text{spor}})^{4-n}(\epsilon_{\text{spor}})^n\binom{4}{n}, \\ &= (1-2\epsilon_{\text{spor}})^4, \\ &= c_{\text{spor}}. \end{aligned} \tag{27}$$

In this calculation, the third equality follows from collapsing a binomial expansion, and the last equality follows from the definition (5) of c_{spor}.

Now consider the propagated-decorrelation textures $T(c_{\text{prop}},1)$. Statistical homogeneity of the textures implies that

$$c_{I,J}=\langle A_{I,J}\cdot A_{I,0}\cdot A_{0,J}\cdot A_{0,0}\rangle. \tag{28}$$

In the propagated-decorrelation textures, the contrast $A_{i,j}$ is equal to the state assignment $a_{i,j}$. Consider the process that generates $a_{I,J}$ from the initial row $a_{0,j}$ and the initial column $a_{i,0}$. The recursion rule of eqn. (2) must be applied IJ times, once for each of the checks $a_{i,j}$ with $1\le i\le I$ and $1\le j\le J$. Let n be the number of times that the product $\langle a_{i,j}\cdot a_{i-1,j}\cdot a_{i,j-1}\cdot a_{i-1,j-1}\rangle$ is *not* equal to 1. Each of these occurrences results in an inversion of the signature of $a_{I,J}$. Thus, the product in eqn. (28) is 1 if n is even, and is -1 if n is odd. It follows that its expected value is

$$\begin{aligned} c_{I,J} &= \sum_{n=0}^{IJ}(-1)^n(1-\epsilon_{\text{prop}})^{IJ-n}(\epsilon_{\text{prop}})^n\binom{IJ}{n}, \\ &= (1-2\epsilon_{\text{prop}})^{IJ}, \\ &= c_{\text{prop}}^{IJ}, \end{aligned} \tag{29}$$

where the last equality follows from the definition (4) of c_{prop}. Finally, the desired result (19) follows multiplication of eqns. (27) and (29), which combines the contribution of $T(c_{\text{prop}},1)$ and $T(1,c_{\text{spor}})$.

Appendix 2: Response of a fourth-power nonlinearity to the isodipole textures

Here we calculate analytically the response of a simple model to the random, even, and odd textures. The model consists of linear summation over $m\times n$ rectangular regions, followed by a fourth-power law given by eqn. (8).

The average response of the nonlinearity (8) to an $m\times n$ region of a texture is the fourth moment of the (signed) contrast summed over that region. This is proportional to

$$M(m,n)=\left\langle\left[\sum_{i=0}^{m-1}\sum_{j=0}^{n-1}A_{i,j}\right]^4\right\rangle. \tag{30}$$

For the random texture, each of the mn quantities $A_{i,j}$ independently assumes the values of $+1$ or -1 with probability 0.5. Thus, the required average is the fourth moment of the binomial distribution on mn objects.

The rth moment of the binomial distribution on k objects, to be denoted $F_r(k)$, is defined by

$$F_r(k)=\sum_{b=0}^{k}2^{-k}(k-2b)^r\binom{k}{b} \tag{31}$$

$F_r(k)$ may be determined from its generating function

$$\begin{aligned} \sum_{r=0}^{\infty}F_r(k)\frac{z^r}{r!} &= \sum_{b=0}^{k}\sum_{r=0}^{\infty}2^{-k}(k-2b)^r\binom{k}{b}\frac{z^r}{r!}, \\ &= \sum_{b=0}^{k}2^{-k}e^{z(k-2b)}\binom{k}{b}, \\ &= 2^{-k}e^{kz}\sum_{b=0}^{k}e^{-2bz}\binom{k}{b}, \\ &= 2^{-k}e^{kz}(1+e^{-2z})^k, \\ &= [\cosh(z)]^k. \end{aligned} \tag{32}$$

A formula for the rth moment of the binomial distribution follows from evaluating the rth derivative (with respect to z) of the generating function (32) at zero:

$$F_2(k)=k, \tag{33}$$

and

$$F_4(k)=3k^2-2k. \tag{34}$$

Thus, for the random texture, the expected value of the fourth moment (30) is

$$\begin{aligned} M_{\text{ran}}(m,n) &= F_4(mn), \\ &= 3m^2n^2-2mn. \end{aligned} \tag{35}$$

For the even and odd textures, we evaluate eqn. (30) by summing over all possible values of the states of the checks in the initial row and column. In both textures, the interior checks are determined by the checks in the initial row and column. We may assume that $a_{0,0}=1$; and corresponding textures with $a_{0,0}=-1$ yield identical contributions to the moment (30). The sporadic error rate ϵ_{spor} is zero, so that the state of each check $a_{i,j}$ is faithfully rendered as $A_{i,j}$ [eqn. (3)].

The even texture is the simpler case. For the even texture, eqn. (7) with $c_{\text{spor}}=1$ and $c_{\text{prop}}=1$ implies that $c_{i,j}=1$. It follows from this perfect long-range correlation [eqn. (6)] and the assumption $A_{0,0}=1$ that

$$A_{i,j}=A_{i,0}A_{0,j}. \tag{36}$$

Therefore, the sum of eqn. (30) factors:

$$M_{\text{even}}(m,n) = \left\langle \left[\sum_{i=0}^{m-1} A_{i,0} \right]^4 \left[\sum_{j=0}^{n-1} A_{0,j} \right]^4 \right\rangle, \\ = \left\langle \left[\sum_{i=0}^{m-1} A_{i,0} \right]^4 \right\rangle \left\langle \left[\sum_{j=0}^{n-1} A_{0,j} \right]^4 \right\rangle. \tag{37}$$

The second equality of eqn. (37) holds because the states in the initial row and the initial column are independent. Each factor in the final expression of eqn. (37) is the fourth moment in a strip of uncorrelated checks. Therefore,

$$M_{\text{even}}(m,n) = F_4(m)F_4(n), \\ = (3m^2 - 2m)(3n^2 - 2n). \tag{38}$$

The calculation of the fourth moment for the odd texture is more elaborate and will only be sketched. For the odd texture, eqn. (7) with $c_{\text{spor}} = 1$ and $c_{\text{prop}} = -1$ implies that $c_{i,j} = (-1)^{ij}$. It follows from this perfect long-range correlation [eqn. (6)] and the assumption $A_{0,0} = 1$ that

$$A_{i,j} = A_{i,0}A_{0,j}(-1)^{ij}. \tag{39}$$

The innermost sum of eqn. (30) no longer factors; however, it can be decomposed as follows:

$$\sum_{i=0}^{m-1}\sum_{j=0}^{n-1} A_{i,j} = \sum_{i=0,\text{even}}^{m-1}\sum_{j=0,\text{even}}^{n-1} A_{i,0}A_{0,j} \\ + \sum_{i=0,\text{even}}^{m-1}\sum_{j=1,\text{odd}}^{n-1} A_{i,0}A_{0,j} \\ + \sum_{i=1,\text{odd}}^{m-1}\sum_{j=0,\text{even}}^{n-1} A_{i,0}A_{0,j} \\ - \sum_{i=1,\text{odd}}^{m-1}\sum_{j=1,\text{odd}}^{n-1} A_{i,0}A_{0,j}. \tag{40}$$

In each term of the decomposition (40), the values of $A_{i,0}$ and $A_{0,j}$ are independent. Evaluation of the fourth moment (30) follows from multinomial expansion of the decomposition (40). We use m_0 to denote the integer part of $(m+1)/2$ (i.e. the number of even integers in $\{0,1,2,\ldots,m\}$), m_1 to denote the integer part of $m/2$, (i.e. the number of odd integers in $\{0,1,2,\ldots,m\}$), and similarly for n_0 and n_1. In the multinomial expansion of eqn. (40), terms with unpaired odd powers of $A_{i,0}$ or $A_{0,j}$ average to zero and may be suppressed. Substitution of the decomposition (40) into the equation for the fourth moment (30) yields

$$\begin{aligned} M_{\text{odd}}(m,n) &= F_4(m_0)F_4(n_0) + F_4(m_0)F_4(n_1) \\ &\quad + F_4(m_1)F_4(n_0) + F_4(m_1)F_4(n_1) \\ &\quad + 6F_4(m_0)F_2(n_0)F_2(n_1) \\ &\quad + 6F_4(m_1)F_2(n_0)F_2(n_1) \\ &\quad + 6F_2(m_0)F_2(m_1)F_4(n_0) \\ &\quad + 6F_2(m_0)F_2(m_1)F_4(n_1) \\ &\quad - 12F_2(m_0)F_2(m_1)F_2(n_0)F_2(n_1), \\ &= [F_4(m_0) + F_4(m_1) + 6F_2(m_0)F_2(m_1)] \\ &\quad \times [F_4(n_0) + F_4(n_1) + 6F_2(n_0)F_2(n_1)] \\ &\quad - 48F_2(m_0)F_2(m_1)F_2(n_0)F_2(n_1). \end{aligned} \tag{41}$$

With the eqns. (33) and (34) for the moments F_k, and the relations $m_0 + m_1 = m$, $n_0 + n_1 = n$, this reduces to

$$M_{\text{odd}}(m,n) = F_4(m)F_4(n) - 48F_2(m_0)F_2(m_1)F_2(n_0)F_2(n_1). \tag{42}$$

Appendix 3: A predicted relationship between antisymmetric responses

The models proposed here implicitly postulate that the response to the basic even texture should be independent of whether it was preceded by an odd texture, or by a random texture. To test this prediction, one cannot simply compare waveforms from the appropriate halves of the stimulus cycles, because the response to one texture likely extends beyond the time during which it is presented (Fig. 2). Nevertheless, observed responses to texture interchange should be equal to combinations of hypothetical basic responses to the even, odd, and random textures. As we now show, this leads to a simple test of the assumption that responses are independent of temporal context.

Denote the hypothetical basic responses to the even, odd, and random textures by $b_e(t)$, $b_o(t)$, and $b_r(t)$. Since the textures are presented with a repetition period P, these functions are also periodic with period P equal to that of the stimulus. Under the hypothesis of "independence of temporal context," the observed raw VEP components should be equal to the sum of two basic responses, one shifted in time by half of the stimulus period, $P/2$. That is,

$$\begin{aligned} v_{e/o}(t) &= b_e(t) + b_o(t - P/2), \\ v_{e/r}(t) &= b_e(t) + b_r(t - P/2), \\ v_{o/r}(t) &= b_o(t) + b_r(t - P/2). \end{aligned} \tag{43}$$

For each of the observed raw signals $v(t)$, the corresponding antisymmetric-response component $v_{\text{anti}}(t)$ is half the difference between the raw response $v(t)$ and its value shifted by half a cycle, $v(t - P/2)$. For example,

$$\begin{aligned} v_{\text{anti};e/o}(t) &= [v_{e/o}(t) - v_{e/o}(t - P/2)]/2, \\ &= [b_e(t) + b_o(t - P/2) - b_e(t - P/2) \\ &\quad - b_o(t - P)]/2, \\ &= [b_e(t) - b_e(t - P/2)]/2 \\ &\quad - [b_o(t) - b_o(t - P/2)]/2, \\ &= b_{\text{anti};e}(t) - b_{\text{anti};o}(t). \end{aligned} \tag{44}$$

Here, the second equality follows from substitution of the eqn. (43) for $v_{e/o}(t)$, and the third equality follows from the fact that the basic responses are periodic with period P. The eqn. (44) states that the observed antisymmetric response components should be equal to the differences of the corresponding antisymmetric components of the hypothetical basic responses $b(t)$.

A relation between antisymmetric responses now follows from combination of eqn. (44) and the analogous equations for the other antisymmetric responses $v_{\text{anti};e/r}(t)$ and $v_{\text{anti};o/r}(t)$:

$$v_{\text{anti};e/o}(t) = v_{\text{anti};e/r}(t) - v_{\text{anti};o/r}(t). \tag{45}$$

Acknowledgments

A portion of this work was presented at the 1987 meeting of the Association for Research in Vision and Ophthalmology, Sarasota, Florida. This work was supported in part by NIH Grants EY1428, EY6871, and NS877.

References

BERGEN, J.R. & JULESZ, B. (1983). Parallel *versus* serial processing in rapid pattern discrimination. *Nature* **303**, 696–698.

DE MONASTERIO, F.M. (1978). Properties of concentrically organized X and Y ganglion cells of macaque monkey retina. *Journal of Neurophysiology* **41**, 1394–1417.

DE VALOIS, R.L., ALBRECHT, D.G. & THORELL, L.G. (1982). Spatial-frequency selectivity of cells in macaque visual cortex. *Vision Research* **22**, 545–559.

DOW, B.M., VAUTIN, R.G. & BAUER, R. (1984). The mapping of visual space onto foveal striate cortex in the macaque monkey. *Journal of Neuroscience* **5**, 890–902.

EMERSON, R.C., CITRON, M., VAUGHN, W.J. & KLEIN, S. (1987). Nonlinear directionally selective subunits in complex cells of cat striate cortex. *Journal of Neurophysiology* **58**, 33–65.

ENROTH-CUGELL, C. & ROBSON, J.G. (1966). The contrast sensitivity of retinal ganglion cells of the cat. *Journal of Physiology* **187**, 517–552.

GAGALOWITZ, A. (1981). A new method for texture fields synthesis: some applications to the study of human vision. *IEEE Transactions on Pattern Analysis and Machine Intelligence* **PAMI-3**, 520–523.

GAGALOWITZ, A. & MA, S.D. (1985). Sequential synthesis of natural textures. *Computer Vision, Graphics, and Image Processing* **30**, 289–315.

HOCHSTEIN, S. & SHAPLEY, R.M. (1976). Linear and nonlinear spatial subunits in Y cat retinal ganglion cells. *Journal of Physiology* **262**, 265–284.

JULESZ, B. (1962). Visual pattern discrimination. *IRE Transactions Inf. Theory* **IT-8**, 84–92.

JULESZ, B. (1981). Textons, the elements of texture perception, and their interactions. *Nature* **290**, 91–97.

JULESZ, B., GILBERT, E. & VICTOR, J.D. (1978). Visual discrimination of textures with identical third-order statistics. *Biological Cybernetics* **31**, 137–140.

KAPLAN, E. & SHAPLEY, R.M. (1982). X and Y cells in the lateral geniculate nucleus of macaque monkeys. *Journal of Physiology* **330**, 125–143.

LEVI, D.M., KLEIN, S.A. & AITSEBAOMO, A.P. (1985). Vernier acuity, crowding, and cortical magnification. *Vision Research* **25**, 963–977.

MILKMAN, N., SCHICK, G., ROSSETTO, M., RATLIFF, F., SHAPLEY, R. & VICTOR, J.D. (1980). A two-dimensional computer-controlled visual stimulator. *Behavioral Research Methods and Instrumentation* **12**, 283–292.

MOVSHON, J.A., THOMPSON, I.D. & TOLHURST, D.J. (1978*a*). Spatial summation in the receptive fields of simple cells in the cat's striate cortex. *Journal of Physiology* **283**, 53–77.

MOVSHON, J.A., THOMPSON, I.D. & TOLHURST, D.J. (1978*b*). Receptive-field organization of complex cells in the cat's striate cortex. *Journal of Physiology* **283**, 79–99.

SPITZER, H. & HOCHSTEIN, S. (1985*a*). Simple- and complex-cell response dependences on stimulation parameters. *Journal of Neurophysiology* **53**, 1244–1265.

SPITZER, H. & HOCHSTEIN, S. (1985*b*). A complex-cell receptive-field model. *Journal of Neurophysiology* **53**, 1266–1286.

VICTOR, J.D. (1985). Complex visual textures as a tool for studying the VEP. *Vision Research* **25**, 1811–1827.

VICTOR, J.D. (1986). Isolation of components due to intracortical processing in the visual evoked potential. *Proceedings of the National Academy of Sciences of the U.S.A.* **83**, 7984–7988.

VICTOR, J.D. (1988). The dynamics of the cat retinal Y cell subunit. *Journal of Physiology* **405**, 289–320.

VICTOR, J.D. & CONTE, M.M. (1987*a*). Visual evoked potentials elicited by simple and complex textures: distinct components with similar scalp topographies. In *Evoked Potentials III: The Third International Evoked Potentials Symposium*, ed. BARBER, C. & BLUM, T. Boston: Butterworths, pp. 183–189.

VICTOR, J.D. & CONTE, M.M. (1987*b*). Local and long-range interactions in pattern processing. (Abstract) *Investigative Ophthalmology and Visual Science* **28** (Suppl.) 362.

VICTOR, J.D. & ZEMON, V. (1985). The human visual evoked potential: analysis of components due to elementary and complex aspects of form. *Vision Research* **25**, 1829–1844.